JVSTB Journal of Vacuum Science & Technology B

Characterization of prototype silicon pitch artifacts fabricated by scanning probe lithography and anisotropic wet etching

F. S.-S. Chien, W.-F. Hsieh, S. Gwo, J. Jun, R. M. Silver, A. E. Vladár, and J. A. Dagata

Citation: Journal of Vacuum Science & Technology B **23**, 66 (2005); doi: 10.1116/1.1835318
View online: http://dx.doi.org/10.1116/1.1835318
View Table of Contents: http://scitation.aip.org/content/avs/journal/jvstb/23/1?ver=pdfcov
Published by the AVS: Science & Technology of Materials, Interfaces, and Processing

Characterization of prototype silicon pitch artifacts fabricated by scanning probe lithography and anisotropic wet etching

F. S.-S. Chien[a)]
Center for Measurement Standards, Hsinchu 300, Taiwan

W.-F. Hsieh
Department of Photonics Engineering, National Chiao-Tung University, Hsinchu 300, Taiwan

S. Gwo
Department of Physics, National Tsing-Hua University, Hsinchu 300, Taiwan

J. Jun, R. M. Silver, A. E. Vladár, and J. A. Dagata
National Institute of Standards and Technology, Gaithersburg, Maryland 20899

(Received 31 August 2004; accepted 25 October 2004; published 28 December 2004)

Scanning probe lithography (SPL) and anisotropic tetra-methyl ammonium hydroxide (TMAH) etching (SPL+TMAH) were used to fabricate a series of one-dimensional prototype pitch structures on (110)-oriented silicon substrates. Overall lateral dimensions of the test structure are 20 μm $\times 80$ μm. Line scales, consisting of 10-μm-long, 100-nm-tall, and 40-nm-wide lines, are observable by optical and scanning electron microscopy (SEM). Etched features were produced with pitches varying from 100 nm to 8 μm. Large-scale pattern placement errors of the SPL tool have been evaluated by analysis of optical image data obtained with a calibrated optical metrology instrument. Small-scale errors were analyzed in the range of 100 nm to 2 μm using SEM. Sources of placement error are discussed and possible methods for minimizing them are presented. The SPL+TMAH process in conjunction with a closed-loop scan control has the precision necessary for repeatable device prototyping in the nanoscale regime. © *2005 American Vacuum Society.*
[DOI: 10.1116/1.1835318]

I. INTRODUCTION

There is a growing need for flexible prototyping of ultrasmall functional device structures in the emerging application areas of nanoelectronics, nanoelectromechanical systems, and photonics. Specific to this last example, silicon-based structures have attracted particular attention for use in monolithically integrated optoelectronic systems,[1] photonic crystals,[2,3] and subwavelength structures[4–6] for which compactness, functional enhancement, and cost reduction are important figures of merit.

Scanning probe lithography (SPL) is a resistless, direct-write method,[7] in which a conductive proximal probe with an applied voltage produces an intense local electric field at the substrate surface, generates an electrochemical reaction within a water meniscus collected from the ambient atmosphere, and results in a controllable oxide pattern. SPL has been successfully demonstrated on a variety of substrates and thin films, including semiconductors,[7] metals,[8–10] and dielectrics.[11] Etch selectivity of the oxide mask[7,12] can be combined with anisotropic wet or dry etching to form a low-cost, highly flexible approach to the fabrication of prototype silicon nanostructures. One-dimensional (1D) and two-dimensional (2D) structures with aspect ratios much greater than 1, i.e., sub-50 nm wide and 100 nm high, have been successfully fabricated in this manner.

Recently, positive-contrast, high-aspect-ratio silicon nanostructures (e.g., ridges) with vertical sidewalls were produced by anisotropic potassium hydroxide (KOH) etching.[13] Cohn *et al.*[14] have proposed tetra-methyl ammonium hydroxide (TMAH) etching as an alternative to KOH etching with advantages of smoothness, selectivity, nontoxicity, and integrated circuit compatibility.[15] From the various silicon nanostructures produced by this process and the compatibility with optical lithography, we conclude that the combination of SPL+TMAH etching is a promising approach to fabricating silicon nanostructures.[16]

A key functional requirement for device prototyping applications is large-scale placement accuracy on the order of 100 μm or more, the typical scan range of most commercially available scanning probe microscopes (SPMs), without loss of feature-width resolution, assumed to be much less than 100 nm. Cohn *et al.* have discussed these requirements recently in terms of the fabrication of visible-wavelength periodic grating filters. Device performance of such filters at visible wavelengths depends crucially on achieving placement accuracy with uncertainties of a few nanometers with respect to nominal line centers. At issue is whether or not commercial SPMs can achieve the tolerances necessary for meaningful fabrication of visible-wavelength, optoelectronic devices. Concern arises because piezoelectric scanners used to raster an SPM probe over a substrate tend to exhibit considerable hysteresis and creep during actuation. Some commercial instruments overcome these limitations by employing a closed-loop scanner, which directly monitors

[a)]Current address: Department of Physics, Tunghai University, Taichung, Taiwan 407.

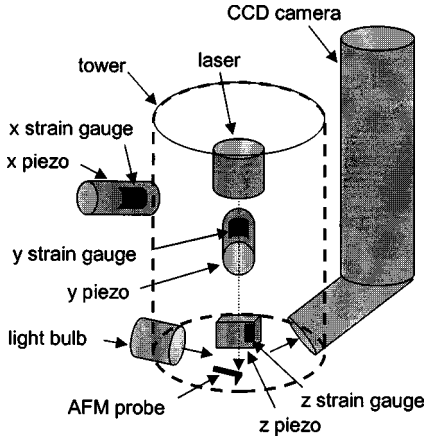

FIG. 1. Schematic of scanning unit of the SPM used in this study, including the tripod closed-loop scanner (feedback circuits not shown), laser, light bulb, and CCD camera. Optical components are a major heat source of the unit and produce thermal drift in the system.

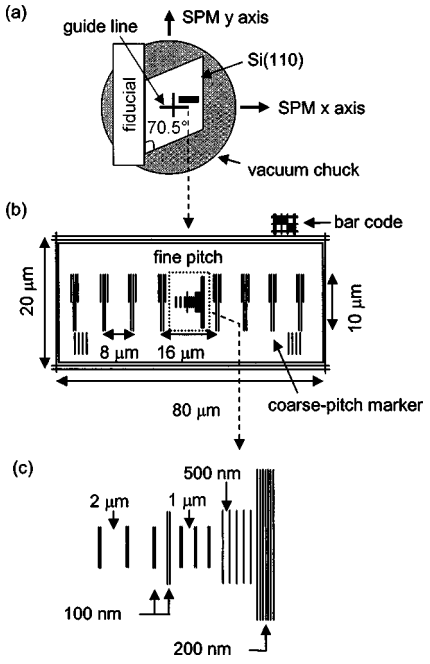

FIG. 2. (a) Alignment of a silicon (110) substrate to the SPM axes. The guide lines scribed into the Si substrate are to aid in locating the pitch. (b) Layout of the 1D pitch structure used in this study (not to scale). It consists of the optically accessible coarse-pitch scale of 8 μm pitch and central SEM-accessible fine-pitch scale. (c) Layout of the fine pitch structure (not to scale) at the central 16 μm region, including the pitches of 100 nm, 200 nm, 500 nm, 1 μm, and 2 μm.

displacement, e.g., optical displacement sensors,[17] capacitive sensors,[18] and interferometers.[19,20] The possibility exists therefore that SPM probe position may be controlled with subnanometer accuracy, meaning that SPL represents a realistic means of nanoscale device prototyping.

In this article, we describe the fabrication of a 1D prototype pitch structure on a Si(110) substrate by the SPL +TMAH process and preliminary results on our efforts to evaluate pattern placement errors arising during fabrication using our SPM instrument. Lateral dimensions of the test structure used in this study are 80-μm-long and 20-μm-wide in order to reveal placement errors over the 100 μm scan range of the SPM. The test structure layout includes a series of pitch markers with nominal values of 8 μm for calibration with an optical metrology instrument maintained at the National Institute of Standards and Technology (NIST), and a series of pitch markers with nominal values from 100 nm to 2 μm for examination by scanning electron microscopy (SEM).

II. EXPERIMENTAL PROCEDURE

A. SPM system

The SPL fabrication tool used in this study is based on a TopoMetrix Accurex II™ SPM system,[21] which employs a tripod-type piezoelectric scanner with integrated strain gauges on all three scan axes to monitor and feedback scanner motion under closed-loop control (Fig. 1). The instrument is isolated from vibration, thermal, and acoustic disturbances by locating it within a humidity-controlled glovebox on a bench-top air table.

Prior qualification of the instrument indicated that the average drift rates of the system after stabilization were 0.017 and 0.083 nm/s in the *X*-fast and *Y*-slow scan directions, respectively. The reason for these disparate drift rates can be appreciated by examining the mechanical loop of the SPM: The scanner tower sits upon a steel beam (not shown), 200 mm × 80 mm × 20 mm (length, width, thickness), with heat sources consisting of a stepper motor, light bulb, laser and preamplifier, and most significantly a CCD camera mounted directly to the right of the scanner tower. Energy dissipation along the long axis of the system produces a thermal gradient along the beam into the system base and, thus, greater drift in that direction. In the present work, we report on analysis of 1D pitch structures which were patterned along the *Y* axis only. We note, however, that in other work highly periodic 2D grid structures have been produced as well, despite the greater *Y*-axis drift. This is because even at 2 μm/s patterning, the drift of the line center is only 4 nm over the full 100 μm scan range of the SPM, which is only about 10% of the SPL-oxide line width.

B. Fabrication of 1D pitch structures

Test structures were prepared from (110)-oriented silicon wafers, with resistivity between 1 and 20 Ω cm, by cleaving along {111} planes to produce parallelogram-shaped chips from the wafer [Fig. 2(a)]. Guide lines for locating the SPL patterned features were scribed into the substrate and the surface was prepared for SPL by ultrasonic cleaning in acetone, isopropyl alcohol, and deionized (DI) water, followed by removal of the native oxide by dipping in 2% HF for 30 s, and a final brief rinse in DI water. Precise alignment of the cleaved {111} edge of the silicon sample to the *X*–*Y* axes of the SPM reference frame was achieved by orienting a fiducial edge onto the vacuum chuck. Accuracy of this alignment was determined by inserting a previously TMAH-etched sili-

con (110) sample and verifying that the angular error between the microscope *Y* axis and silicon {111} direction was a few tenths of a degree or less.

For this study, SPL was performed in contact mode and subsequent imaging of the latent oxide patterns was performed in noncontact mode. Contact-mode cantilevers coated with conductive tungsten carbide from MikroMasch were used.[22] Typical force constants and resonance frequencies were 0.95 N/m and 105 kHz, respectively. For SPL, a bias of 9 to 12 V was applied to the sample, established by initial test patterning with a particular cantilever. Lines were formed using a writing speed of 2 μm/s. Pattern generation was controlled by running SPMLAB[21] and TOPOLITH[21] programs simultaneously on a Windows™ computer. Input files used by the TOPOLITH software to generate the test structure were created and validated using a spreadsheet program.

The pattern layout for the 1D test structure, including an optically accessible coarse-pitch scale and an SEM-accessible fine-pitch scale, is shown in Fig. 2(b). The coarse-pitch scale consists of an array of markers with a nominal 8 μm pitch spanning the width of the structure. These markers are visible in an optical microscope (OM) after TMAH etching. Note that the 8 μm pitch markers are composed of a series of four parallel, sub-50-nm-wide lines, and that the inner pair extends several micrometers beyond the outer pair. Individual lines are not resolved in an OM, so that the optical profile resulting from the unresolved inner pair of lines was used in our pitch analysis. The center of the test structure contains a fine-pitch scale intended for SEM image analysis [Fig. 2(c)]. Nominal pitch values from 100 nm to 2 μm are represented. The sequence used to generate the pattern is as follows. First, the TOPOLITH program patterned the fine-pitch scale at the origin of the SPM reference frame; i.e., zero applied voltage on the *X* and *Y* scanner piezos. Next, 8 μm pitch markers were patterned at locations along the *X* axis from −32 to +32 μm. Finally, a 20 μm × 80 μm box surrounding the markers was patterned and a bar code identifier was written outside the upper right-hand corner of the box. Patterning of one test structure fabricated for this study took about 40 min at the 2 μm/s scan speed, although much higher scan speeds have been used successfully as well.

After SPL oxide patterning, substrates were etched for 40 s in a TMAH-isopropyl alcohol (IPA) solution maintained at 60 °C, and then rinsed briefly in DI water. [IPA is added to 25 wt % TMAH to achieve a solution of 83 parts of TMAH + 17 parts of IPA by volume. According to our data, the etch rate was reduced by about 55% for silicon {110} planes by the use of IPA.] This solution produced smooth silicon features, with a height between 100 and 150 nm, determined from SPM images, and linewidth about 40 nm, estimated at the midpoint of edge-enhanced, secondary-electron intensity maxima in top-down SEM images.

It is important to understand the role of the 2-nm- to 3-nm-thick SPM-oxide pattern in the context of anisotropic silicon etching. Etching anisotropy at the nanometer scale is different from its conventional behavior at larger length scales. The SPL oxide pattern imposes an "initial condition" on the etch front that resists an early isotropic etching phase long enough to allow the system to find geometrically stable planes such as {111}. Conversely, the terminal geometry is affected by the residual thickness and stability of the SPL-oxide pattern in conjunction with the stability of the {111} planes. The etching is a diffusion-limited reaction within the local region of gap between lines, so that the etch front is preferential in the direction where the oxide pattern and {111} planes are less correlated.[23]

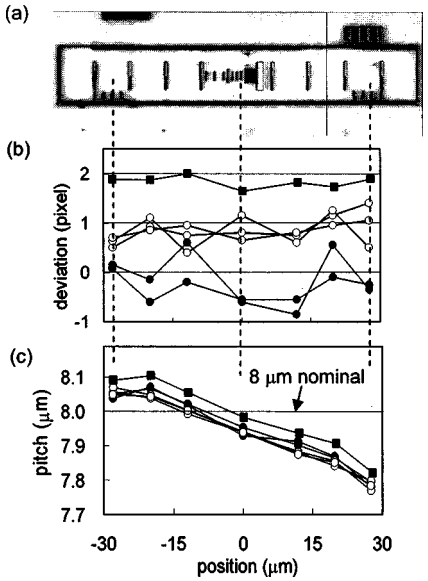

FIG. 3. (a) Overlapping optical images of an etched structure. (b) Plot of pitch deviation vs. position between optical measurements obtained on each of six samples on different days (Samples: ● A_1; ○ A_2; ■ A_3). The A_2 and A_3 are offset by +1 and +2, respectively, for clarity. (c) Optical pitch measurements compared to nominal 8 μm value (horizontal solid line). The center pitch value has been divided by 2 to aid interpretation.

We find that we can routinely pattern and etch constant-width lines that are many tens of micrometers long, clear evidence that alignment of the silicon {111} substrate to the *Y* axis of the SPM is within the tolerance required for etching. Three samples, produced on separate days, were denoted as A_1, A_2, and A_3, on which we fabricated a total of six test structures (one on A_1, three on A_2, and two on A_3).

III. DATA ANALYSIS OF OPTICAL AND SEM IMAGES

A. Optical analysis of coarse-pitch scales

Optical images of all six test structures were obtained using an OM-based dimension metrology instrument maintained at NIST. Design of this instrument and data analysis methods are described elsewhere.[24] Images were recorded at 50x magnification using a calibrated-pixel CCD camera. [All measurements described in this work are for the purpose of qualifying the SPL process and are not intended to be traceable.] Since the field of view recorded in a single image is approximately 50 μm across at 50x magnification, three overlapping data files were required to analyze each 80-μm pitch structure [Fig. 3(a)]. Each image contains 1024 pixels along the (horizontal) *X* axis. Previous qualification of the

instrument yielded an average pixel length corresponding to 42 nm. In addition, each structure was imaged with the sample oriented at 0° and 180° relative to the instrument axes to identify and eliminate possible calibration bias of the CCD camera. Statistical deviations were found to be insignificant and all subsequent data were a simple average of the combined data files. Random variations were eliminated by imaging the entire series of test structures on multiple occasions.

Three algorithms for determining the line center and/or pitch were used: (1) Centroid method. An integration of the area beneath the line profile was performed and the line center was associated with the position at which the area reaches half its total value. Both a line center and a pitch are determined. (2) Cross-correlation method. Each line profile was translated to a position overlapping a reference line such that the sum of the square difference of the two heights is a minimum. Only a pitch measurement is obtained. (3) Folded center method. A portion of a line profile is reflected onto its opposite slope and again the line center is determined to be that position for which the sum of the square difference of the two heights is a minimum. In a few cases, the cross-correlation results from method 2 are so flat that the pitch is not precisely determined. All three methods produced very similar results for the sets of optical data. All pitch results reported in this work are a simple average of all three methods.

Figure 3(b) presents a plot of the relative deviation of pitch measurements for sets of images taken several weeks apart. Note that values for the A_2 and A_3, datasets are offset by $+1$ and $+2$, respectively, for display clarity. The plot indicates that the optical measurement produces errors of ± 0.5 pixels, or ± 21 nm, as determined from previous calibration of the CCD camera array. Optical pitch measurements appear in Fig. 3(c). These values for the six structures should be compared to the horizontal line that represents the nominal 8 μm pitch value. Note that at the center of the structure the nominal pitch is actually 16 μm and we have simply divided this value by 2 in the figure to aid data interpretation.

There are two trends that are evident in Fig. 3(c). First, there is a systematic linear decrease in pitch from left to right. The same trend is consistently reproduced in each dataset. Second, an apparently random multiplier, representing a fraction of a pixel, shifts the linear curve vertically. It is strongly correlated to the day on which the structures were fabricated. Note that in absolute terms the actual pitch produced in our SPL tool at the coordinate center of the SPM is 0.6% less than the nominal value: 7.95 μm rather than 8 μm. To the left and right of center, $\sim \pm 30$ μm, placement error increases from 1% to 2%.

B. SEM analysis of fine-pitch scales

SEM imaging was performed in a field-emission instrument[25] with a 5 kV accelerating voltage and 5.2 mm working distance. Since magnification is a sensitive function of the working distance in a SEM and repeatability of the working distance can be controlled to only a few percent, pitch measurements of an identical structure from SEM images taken on different days were fitted to an overall magnification function. A SEM magnification error of approximately 5% was obtained, consistent with expectation.

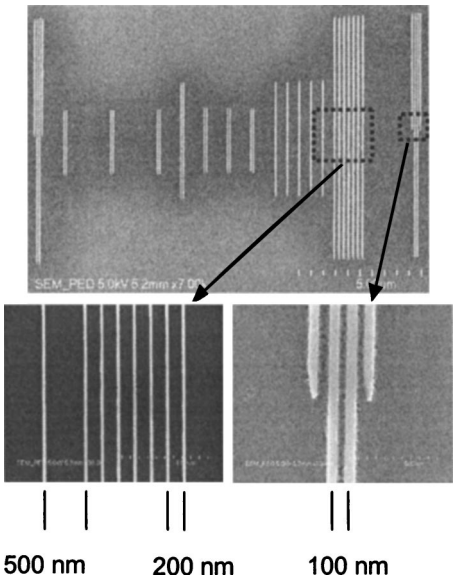

FIG. 4. SEM images of the fine-pitch scale of sample A_1 and close-ups of the submicrometer pitch regions.

SEM images were collected at a magnification of 7000, with data files containing 2048 pixels along the *X* axis. This provides sufficient data points with nominally 7 nm pixel size for line profile analysis, while at the same time obtaining both the fine-pitch features as well as the nominal 16 μm markers previously calibrated by optical means. SEM images taken of the fine-pitch region of sample A_1, shown in the Fig. 2(c) schematic, are shown in Fig. 4. Higher magnification images (insets) demonstrate that highly uniform silicon lines of sub-50-nm width and 100 nm pitch can be achieved with the SPL+TMAH process.

Pronounced asymmetry at isolated line edges can occur in SEM images since the secondary-electron emission is enhanced at isolated sidewalls relative to closely spaced features. Monte-Carlo modeling of electron trajectories is needed in order to obtain a correct location of these edges. For the present analysis, our primary concern lies in transferring the OM calibration to the fine-pitch scale. Since the major uncertainty arises from CCD calibration, and this is greater than the uncertainty resulting from edge effect in SEM images, it is justified to assume that such effects are a small perturbation to our methods for pitch determination. As in the OM image analysis, all four methods produced very similar line center locations for the SEM data, so that we use a simple average of all four results.

Figure 5 presents (a) correlated SEM image, (b) pitch-error information, and (c) placement-error information across the 16 μm center region of the test structure. As noted earlier, the 8 μm optical marker array was patterned after the intervening fine-pitch scale was patterned. Thus, the fine-pitch

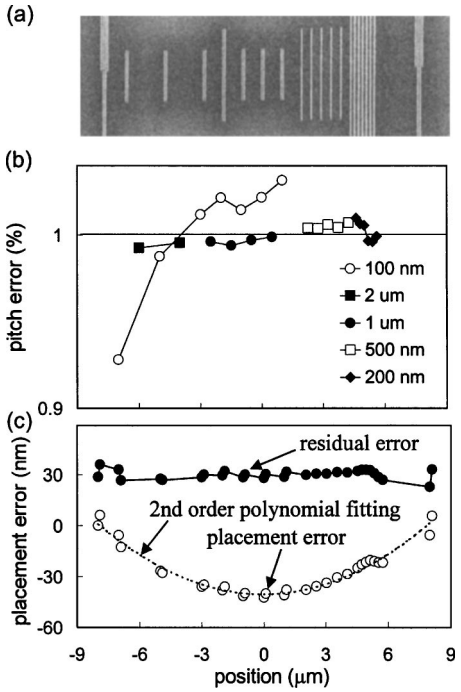

FIG. 5. (a) SEM image of the fine-pitch scale of sample A_1 (detail) aligned with (b) the plot of pitch error (difference between experimental and nominal pitches) vs position, and (c) the plot of the placement error (difference between experimental and nominal placements) with second-order polynomial fitting and the residual error (difference between experimental placement and the fitting) vs. position. The residual error is offset by +30 nm for clarity.

lines may be offset with respect to the 16 μm pitch markers due to SPM drift. A three-parameter fit allowed us to determine the relative translational and/or magnification errors during fabrication. Indeed, a small drift-related translation of the two sets of scales as well as a slight difference in magnification can be observed.

Figure 5(b) reveals that the deviation of pitch values from the nominal are within 1% for scales between 200 nm and 2 μm, with a slight drift upward from left to right. Deviation of the 100 nm scale markers are well above 1% because they are sensitive to drift in the SPM as well TMAH etching conditions. To analyze the placement error [Fig. 5(c)], we have corrected the drift-related translation of SPM and the magnification error of SEM. The placement error is the difference of the experiment to nominal placements with the characterized 16 μm pitch markers as references on both ends. A bowing of the placement [Fig. 5(c)] in the fine-pitch data was found which differs qualitatively from the linear trend of the coarse-pitch measurements. The error is less than 40 nm across the 16 μm central region of the test structure and is described by a second-order polynomial fitting. The residual errors are within ±5 nm from the fitting.

IV. DISCUSSION

The SPL+TMAH process is a reliable method for producing silicon features with sub-50 nm linewidth with smooth sidewalls over scan ranges accessible with most commercial SPMs. Furthermore, we have demonstrated repeatable fabrication of etched silicon features with 100 nm. Because SPL oxidation is a local reaction that does not require high energies, charged particles, or optical interference through a resist, difficult control issues such as proximity effects or phase shifting encountered in traditional lithography can be avoided at the device prototyping stage. For example, it is difficult to produce highly uniform lines by traditional e-beam lithography and dry etching, since scattering of energetic charged particles for the resist exposure and dynamic bombardment of radicals for etching silicon are involved. Linewidth uniformity becomes crucial for feature widths below 100 nm. The SPL+TMAH process produces highly uniform, sub-50 nm features defined by vertical Si(111) sidewalls resistant to gentle TMAH etching.[16] The estimated roughness of the sidewalls is less than 5 nm. These are important features in the consideration of the SPL +TMAH process for applications in nanophotonic device fabrication.

Centroids for each line profile in the OM images were assessed using three algorithms. The linear decrease in pitch identified from the optical images indicates the existence of a systematic placement error across the 100 μm scan range of the SPM, ranging from −2% to +1%. This error results from the nonideal response of the closed-loop scanner. By including an error-correction function into the generation of the TOPOLITH input files, it should be possible to further reduce systematic placement errors over the scan range of the instrument by an order of magnitude. A true error-correction function would be obtained after certain iterations of the process from patterning to characterizing. We have presented a scheme to characterize, analyze, and correct the placement errors of a SPM could be an operational rule applied to most commercial SPMs to improve their placement accuracy.

The day-to-day random multiplier error is approximately ±0.4%, probably arising from the thermal gradients in the mechanical loop produced by the CCD camera, bulb and laser diode mounted close to the scanner. Future efforts to remove heat sources, especially the CCD camera during patterning, and developing standardized equilibration procedures during SPM setup are two steps that are expected to improve overall placement error to the level of 0.1%, which will satisfy the anticipated accuracy requirements for nanophotonic device prototyping.

We notice that pitch accuracy deteriorates when the pitch of successive lines varies, as illustrated on the left-hand side of Fig. 5(b), in which lines alternate from between 100 nm and 1 μm to 2 μm. On the other hand, the error appears to be reduced if several successive lines of the same pitch are written, as seen in the groups of lines with making up the 200 nm and 500 nm scales on the right hand side of Fig. 5(b). This behavior suggests that the scanner is not stable immediately after the pitch is varied because of piezo creep, and that longer settling times or blanking lines may be required in order for the scanner to exhibit more reproducible position in

the 100 nm regime. The throughput will inevitably decrease when placement accuracy in the range of 100 nm are involved.

The second-order placement error in Fig. 5(c) could arise from two possible sources: (a) the coupling between SPM scanner axes and (b) the aberration of electron-beam deflection. Both are known sources of error with a magnitude on the order of what we obtain in this analysis. At this moment, we do not have enough evidence to distinguish the source of this error. Further effort is needed to clarify and reduce the error, as the magnitude of the error is significant for placement accuracy below 100 nm. Performance of SPL will vary with SPM design, and accordingly placement errors will arise from different sources. However, SPMs equipped with adequate closed-loop scanner control should be capable of executing SPL to a level of placement accuracy similar to the instrument described here. Moreover, the same approach toward evaluating the pattern-generating system from the range of 100 μm down to 100 nm can be adopted and error-correction functions implemented during the preparation of lithography input files.

V. CONCLUSION

We have produced a series of 20 μm $\times$ 80 μm, 1D prototype pitch artifacts with uniform linewidth below 50 nm using the process of SPL+TMAH etching. Pattern placement accuracy, a key requirement for nanodevice applications, has been evaluated by image analysis of coarse- and fine-pitch scales from 8 μm down to 100 nm using a calibrated optical metrology instrument and SEM. For the coarse-pitch scale, we found a systematic linear decrease in pitch, accounted for by the nonideal response of the closed-loop scanner. This produces a placement error of 0.6% at the center of the SPM scan coordinates and 1% to 2% over $\pm$ 30 μm. A probable source of day-to-day variations is related to thermal drift of the SPM. For the fine-pitch scale, deviation of pitch measurements from the nominal value was less than 1% in the range of 200 nm to 2 μm, and placement error below 100 nm requires further investigation.

ACKNOWLEDGMENTS

Support for this work from Steven Knight and Jack Martinez of the NIST Office of Microelectronics Programs is gratefully acknowledged.

[1]*Materials and Devices for Silicon-Based Optoelectronics*, edited by A. Polman, S. Coffa, and R. Soref (Material Research Society, Warrendale, 1998).
[2]J. S. Foresi, P. R. Villeneuve, J. Ferrera, E. R. Thoen, G. Steinmeyer, S. Fan, J. D. Joannopoulos, L. C. Kimerling, H. I. Smith, and E. P. Ippen, Nature (London) **390**, 143 (1997).
[3]T. Zijlstra, E. van der Drift, M. J. A. de Dood, E. Snoeks, and A. Polman, J. Vac. Sci. Technol. B **17**, 2734 (1999).
[4]D. L. Brundrett, E. N. Glytsis, and T. K. Gaylord, Opt. Lett. **23**, 700 (1998).
[5]P. Lalanne and G. M. Morris, Nanotechnology **8**, 53 (1997).
[6]Y. Kanamori, K. Hane, H. Sai, and H. Yugami, Appl. Phys. Lett. **78**, 142 (2001).
[7]J. A. Dagata, J. Schneir, H. H. Harary, C. J. Evans, M. T. Postek, and J. Bennett, Appl. Phys. Lett. **56**, 2001 (1990); J. A. Dagata, Science **270**, 1625 (1995), and references therein.
[8]H. Sugimura, T. Uchida, N. Kitamura, and H. Masuhara, J. Phys. Chem. **98**, 4352 (1994).
[9]E. S. Snow, D. Park, and P. M. Campbell, Appl. Phys. Lett. **69**, 269 (1996).
[10]S. Gwo, C.-L. Yeh, P.-F. Chen, Y.-C. Chou, T. T. Chen, T.-S. Chao, S.-F. Hu, and T.-Y. Huang, Appl. Phys. Lett. **74**, 1090 (1999).
[11]F. S.-S. Chien, J.-W. Chang, S.-W. Lin, Y.-C. Chou, T. T. Chen, S. Gwo, T.-S. Chao, and W.-F. Hsieh, Appl. Phys. Lett. **76**, 360 (2000).
[12]E. S. Snow, W. H. Juan, S. W. Pang, and P. M. Campbell, Appl. Phys. Lett. **66**, 1729 (1995).
[13]F. S.-S. Chien, C.-L. Wu, Y.-C. Chou, T. T. Chen, S. Gwo, and W.-F. Hsieh, Appl. Phys. Lett. **75**, 2429 (1999).
[14]R. W. Cohn, S. F. Lyuksyutov, K. M. Walsh, and M. M. Crain, Opt. Rev. **6**, 345 (1999).
[15]O. Tabata, R. Asahi, H. Funabashi, K. Shimaoka, and S. Sugiyama, Sens. Actuators, A **34**, 51 (1992).
[16]F. S.-S. Chien, W.-F. Hsieh, S. Gwo, A. E. Vladar, and J. A. Dagata, J. Appl. Phys. **91**, 10044 (2002).
[17]R. C. Barrett and C. F. Quate, Rev. Sci. Instrum. **62**, 1393 (1991).
[18]J. E. Griffith, G. L. Miller, C. A. Green, D. A. Grigg, and P. E. Russell, J. Vac. Sci. Technol. B **8**, 2023 (1990).
[19]J. Schneir, T. H. McWaid, J. Alexander, and B. P. Wilfley, J. Vac. Sci. Technol. B **12**, 3561 (1994).
[20]S. Gonda, T. Doi, T. Kurosawa, Y. Tanimura, N. Hisata, T. Yamagishi, H. Fujimoto, and H. Yukawa, Rev. Sci. Instrum. **70**, 3362 (1999).
[21]TopoMetrix (Santa Clara, CA), Accurex II™. Certain commercial equipment is identified in this report to adequately describe the experimental procedure. Such identification does not imply recommendation or endorsement by the National Institute of Standards and Technology, nor does it imply that the equipment identified is necessarily the best available for the purpose.
[22]MikroMasch (Tallinn, Estonia). See disclaimer in Ref. 21.
[23]B. Legrand and D. Stievenard, Appl. Phys. Lett. **74**, 4049 (1999); **76**, 1018 (2000).
[24]R. M. Silver, J. Jun, E. Kornegay, and R. Morton, Proc. SPIE **4344**, 515 (2001), and references therein.
[25]Hitachi S-4700 cold-field scanning electron microscope. See disclaimer in Ref. 21.